Effective Radius of Ice Cloud Particle Populations Derived from Aircraft Probes

ANDREW J. HEYMSFIELD, CARL SCHMITT, AND AARON BANSEMER

National Center for Atmospheric Research, Boulder, Colorado*

GERD-JAN VAN ZADELHOFF

Koninklijk Nederlands Meteorologisch Instituut, De Bilt, Netherlands

MATTHEW J. MCGILL

NASA Goddard Space Flight Center, Greenbelt, Maryland

CYNTHIA TWOHY

College of Oceanic and Atmospheric Sciences, Oregon State University, Corvallis, Oregon

DARREL BAUMGARDNER

Centro de Ciencias de la Atmosfera, Universidad Nacional Autonoma de Mexico, Mexico, Mexico

(Manuscript received 25 February 2005, in final form 1 September 2005)

ABSTRACT

The effective radius (r_e) is a crucial variable in representing the radiative properties of cloud layers in general circulation models. This parameter is proportional to the condensed water content (CWC) divided by the extinction (σ). For ice cloud layers, parameterizations for r_e have been developed from aircraft in situ measurements 1) indirectly, using data obtained from particle spectrometer probes and assumptions or observations about particle shape and mass to get the ice water content (IWC) and area to get σ, and recently 2) from probes that derive IWC and σ more directly, referred to as the direct approach, even though the extinction is not measured directly.

This study compares [IWC/σ] derived from the two methods using datasets acquired from comparable instruments on two aircraft, one sampling clouds at midlevels and the other at upper levels during the Cirrus Regional Study of Tropical Anvils and Cirrus Layers (CRYSTAL) Florida Area Cirrus Experiment (FACE) field program in Florida in 2002. A penetration by one of the aircraft into a cold midlatitude orographic wave cloud composed of small particles is further evaluated. The σ and IWC derived by each method are compared and evaluated in different ways for each aircraft dataset. Direct measurements of σ exceed those derived indirectly by a factor of 2–2.5. The IWC probes, relying on ice sublimation, appear to measure accurately except when the IWC is high or the particles too large to sublimate completely during the short transit time through the probe. The IWC estimated from the particle probes are accurate when direct measurements are available to provide constraints and give useful information in high IWC/large particle situations.

Because of the discrepancy in σ estimates between the direct and indirect approaches, there is a factor of 2–3 difference in [IWC/σ] between them. Although there are significant uncertainties involved in its use, comparisons with several independent data sources suggest that the indirect method is the more accurate of the two approaches. However, experiments are needed to resolve the source of the discrepancy in σ.

* The National Center for Atmospheric Research is sponsored by the National Science Foundation.

Corresponding author address: Andrew Heymsfield, NCAR, P.O. Box 3000, Boulder, CO 80307.
E-mail: heyms1@ncar.ucar.edu

1. Introduction

Better representations of ice cloud microphysical properties are needed to improve representations of cloud radiative properties in general circulation models (GCMs). Researchers are concerned with the relationship between the ice water content (IWC) and the ice cloud effective radius (r_e). The IWC is a prognostic variable in modern GCMs. The r_e for ice clouds is a fundamental determinant of a cloud's radiative properties. It is proportional to the ratio of IWC to the extinction coefficient (σ), and is almost always specified from empirically derived relationships because factors that influence σ-crystal shape and details of the particle size distributions (PSDs) can vary widely from one cloud to another. Advances in the treatment of ice cloud radiative properties in GCMs will require reliable estimates of r_e and its representation in terms of cloud type, temperature, and microphysical properties.

For obtaining r_e for ice clouds, at least three methods have been used: in situ data, from PSD and ice particle habit information; direct measurement of IWC and σ; and from remote sensing using coincident lidar and radar measurements. Although satellite remote sensing measurements have been used to deduce r_e, the parameterizations have been developed using one or more of the other methods.

The first method uses PSD measured from two-dimensional (2D) imaging probes and assumptions about the dominant particle habits (Heymsfield and Platt 1984) or the actual particle areas measured by the 2D probe (Heymsfield and McFarquhar 1996; Boudala et al. 2002). Below the 2D probe's size detection limit of about 50 μm, PSD are often taken to be that measured by a one-dimensional forward scattering spectrometer probe (FSSP) (Ivanova et al. 2001) or from a video ice particle sampler (McFarquhar and Heymsfield 1996). Except when all particles are smaller than a few hundred microns, FSSP concentrations may be overestimated because of particle breakup on the probe's inlet (Field et al. 2003). The 2D probe may also mis-size and undercount particles smaller than 125 μm (Korolev et al. 1998; Strapp et al. 2001). Shattering of particles on the tips of the imaging probes when large particles above several millmeters are present can artificially enhance the concentrations of small particles (Field et al. 2006, manuscript submitted to *J. Atmos. Oceanic Technol.;* hereafter FHB). The IWC is estimated from the combined PSD using relationships between particle mass and diameter (mass dimensional relationships). Extinction is derived from twice the total cross-sectional area of the particle population. Method 2 uses independent measurements of IWC and σ, an approach

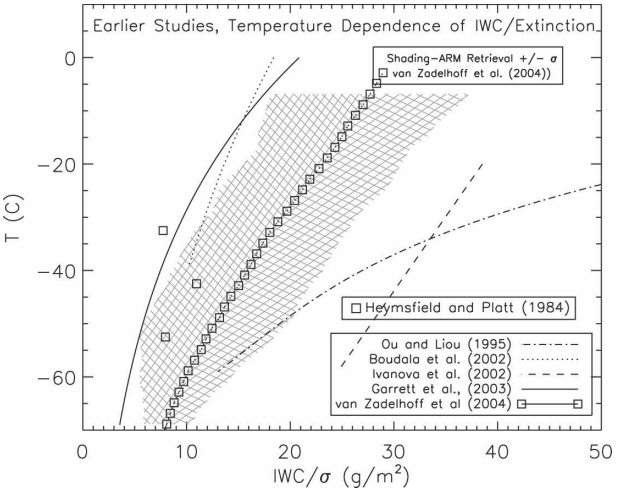

FIG. 1. Estimates of the ratio of ice water content to extinction from earlier studies.

pioneered by Korolev et al. (1999, 2001). Here, IWC is obtained from one of the new evaporator devices ["Harvard"; Weinstock et al. (1994); Weinstock 2005, unpublished manuscript], counterflow virtual impactor [CVI; Twohy et al. (1997)]. Over a large size range, the cloud integrating nephelometer (CIN; Gerber et al. 2000) derives the visible extinction coefficient, independent of ice crystal size and shape. The CIN active scattering volume is sandwiched between two wings in the form of a split ellipsoid to minimize interaction of cloud particles with the probe housing. The CIN measures the light scattered in the forward and backward directions and the extinction coefficient is calculated based on assumptions about the particle shape (Gerber et al. 2000). It is not a transmissometer, which would provide a direct measurement. In the third method, lidar backscatter measurements are used to derive σ, and radar and lidar are used together to derive IWC (e.g., Donovan 2003; van Zadelhoff et al. 2004).

Figure 1 shows the temperature dependence of [IWC/σ] derived from the three methods, in clouds covering geographical areas from low latitudes to the Arctic. Although each method shows an increase in [IWC/σ] with temperature, for any given temperature the different methods give widely differing results. This is partially geographic and cloud type related: in nonconvective midlatitude clouds studied by Heymsfield and Platt (1984), Ou and Liou (1995), and Ivanova et al. (2001); in nonconvective high-latitude clouds by Boudala et al. (2002); and mostly convectively generated, low-latitude clouds by Garrett et al. (2003). From a huge dataset, the remote sensing method spans the range derived from the PSD. In contrast, the direct

TABLE 1. Temperatures sampled from the various datasets used in this study.

	Sampling temperatures							
	Percent samples in temperature interval (°C)							
No. of 5-s samples	<−75	−75 to −65	−65 to −55	−55 to −45	−45 to −35	−35 to −25	−25 to −15	−15 to 0
				WB57F CRYSTAL-FACE				
4463	1.1	34.8	59.9	2.5	<1	<1	0	0
				Citation CRYSTAL-FACE				
11 580	0	<0.1	9.2	20.2	25.2	18.3	8.5	13.8
				CEPEX				
53	0	0	1.9	34.0	66.0	1.9	0	0
				Replicator FIRE-2				
109 (layers)	0	0	10.1	33.0	34.9	16.5	3.7	0

measurement approach yields values lower than those derived from either of the other methods.

The direct measurement approach is appealing in that it does not involve assumptions about ice particle mass and removes errors involved in the measurement of large (2D probe size) and small (FSSP size) particles (Korolev et al. 1999, 2001). Given also that it is the newest of the approaches, it is likely to be adopted by the GCM community and will be used in future assessments of the role of ice clouds in climate change scenarios, but with this method, derived [IWC/σ] values are radically lower than those obtained by the other approaches.

To better understand the current discrepancies and to produce more reliable estimates of r_e in the future, this paper looks into the validity and use of in situ measurements. We compare particle probe and direct measurements, assessing their accuracy using data from the same aircraft. The Cirrus Regional Study of Tropical Anvils and Cirrus Layers (CRYSTAL) Florida Area Cirrus Experiment (FACE) observations are presented in section 2 and observations in an orographic wave cloud are presented in section 3. Conclusions and recommendations are given in section 4.

2. Observations from CRYSTAL-FACE

The effective radius of an ice particle population is composed of two variables: extinction (m^{-1}) and the IWC (g m^{-3}). From Fu (1996), the effective radius, r_e (μm), is just 1.27[IWC/σ], and from Garrett et al. (2003) it is 1.65[IWC/σ]. Both σ and IWC are dependent upon the particle size distribution and the ice particle habit. They can be derived from bulk measurements of these variables. They may also be derived indirectly from PSD measurements of small and large particles, ice particle habit information, and assumptions about particle mass and cross-sectional area. It should be noted that it is currently difficult to accurately measure the size distribution of small particles (Field et al. 2003).

Datasets containing direct measurements, PSDs in small and large particles, and habit information were acquired in low-latitude ice cloud layers. The data were obtained by the University of North Dakota Citation and the National Aeronautics and Space Administration (NASA) WB57F aircraft, in southern Florida and off the coast of Central America during CRYSTAL-FACE during July 2002. The Citation observations focused on warmer temperatures than the WB57F. The CRYSTAL-FACE sampling temperatures and numbers of samples are presented in Table 1.

These observations provide one of the first opportunities to compare and evaluate σ and IWC obtained both directly and indirectly in low-latitude clouds that may be important to the earth's radiation budget. In this section, we examine 11 Citation and 7 WB57F flights from CRYSTAL-FACE and evaluate them based on ancillary observations. Small particles contribute a major portion of the extinction in ice clouds (e.g., Ivanova et al. 2001) and we begin by evaluating the small particle probes. The estimates of σ are then examined, followed by an assessment of the IWC measurements, and finally by an evaluation of the ratio [IWC/σ].

On 9 July 2002, data were acquired by the Citation in supercooled regions at temperatures near −6°C composed almost exclusively of cloud droplets. The performance of the forward scattering spectrometer probe (FSSP), the probe used to obtain PSDs for "small" particles (about 3–45 μm), can be assessed in these liquid water (LW) regions because assumptions about small particle shapes are not required. Indices of refraction and other sizing concerns are not an issue. The FSSP was calibrated both before and after CRYSTAL-FACE, and the postproject calibration indicated the possibility of some undersizing due to dirty optics. A comparison of the ratio of σ from the indirect to direct

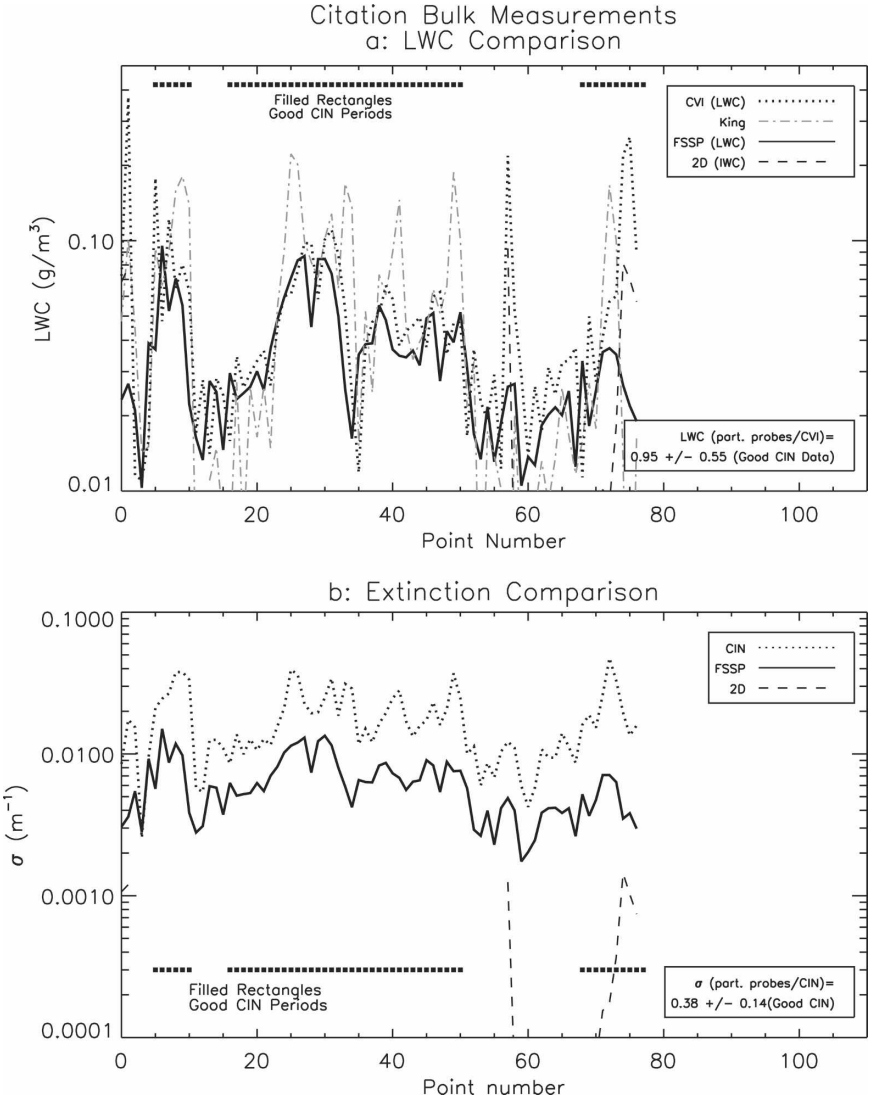

FIG. 2. Observations from Citation aircraft in liquid water regions on 9 Jul 2002 during CRYSTAL-FACE. The broad time range used in (a) was 64 820 to 69 350 UTC seconds, when icing was not affecting the CIN measurements. In the figure, data are plotted for those times during the above time interval when the King LWC corrected for drift exceeded 0.05 g m^{-3}. (a) Liquid water content derived from the FSSP compared to those measured by the CVI and the King probe. Mean ratio for the periods of good CIN data, and for the entire flight where LW was observed, are shown in the lower right. (b) Comparison of extinction derived from FSSP to measurements from the CIN probe.

approaches over the course of the field program indicates no tendency for the FSSP to undersize. In the LW regions, drizzle was detected by the cloud particle imager probe on board the Citation, as were at times some larger needle-shaped crystals.

Figure 2a compares the liquid water content (LWC) obtained by integrating the FSSP PSDs and an IWC in 2DC probe sizes (assuming the large particles are ice) with the condensed water content (CWC, LWC + IWC) measured by the CVI probe. A thorough discussion of the CVI's measurement technique and its accuracy are given in the appendix. Times were identified on 9 July when the LWC from a King LWC probe was greater than 0.05 g m^{-3} and when liquid water was simultaneously detected by a Rosemount icing detector. This subset of times was further restricted to those periods early on in the flight where the CIN probe was operating normally, that is, when the probe was not impaired significantly by icing conditions. [Icing is inferred from the ratio of the scattering in the back to the

forward channel.] Problems showed up later in the flight. The "good" periods are identified in Fig. 2a and are plotted in the comparison. The IWC from the large particle probe was derived using the CRYSTAL-FACE density formulation developed by Heymsfield et al. (2004a). As configured on the Citation, the CVI sampled droplets from about 6-μm diameter and is accurate to $\pm$24% for CWC above 0.005 g m^{-3}. On 9 July, the LWC in FSSP sizes below the CVI's size detection threshold was almost always small ($<$0.005 g m^{-3}) compared with the LWC from the CVI. In regions where the large particle probe detects no particles, the CVI and FSSP LWCs are almost the same. The King probe indicated slightly larger values in the regions of peak LWC. CPI data indicated that there were drizzle drops at these times. There is a small time offset not accounted for in the plotted CVI data. As is shown in Fig. 2a, the mean ratio of the CWC from the particle probes and the CVI is nearly unity, for the periods plotted and also for all liquid water periods on the flights. We conclude from this comparison that the FSSP measured the droplet PSD accurately.

Figure 2b gives extinction estimates from the FSSP and from the particle probes, as well as values measured directly by the CIN probe. The extinctions, σ, from the FSSP and CIN have almost the same patterns and magnitudes, but as indicated from the ratio shown in the lower-right corner, σ for the CIN is two-and-a-half times larger than for the FSSP, suggesting that the CIN is overestimating σ by a factor of about 2.5 because the LWCs from the FSSP appear to be correct.

Figures 3a and 3b give the broader Citation extinction dataset from ice regions, noting that σ (FSSP + 2DC)/CIN is again a mean of about 0.38 (bottom left), indicating that the CIN probe gives larger values of σ than the FSSP in ice as well as liquid. Figures 4a and 4b give the WB57F extinction data from the Droplet Measurement Technologies' Cloud and Aerosol Spectrometer (CAS) and the Cloud Imaging Probe (CIP), replacing FSSP and the 2DC. The discrepancy in σ also exists.

In regions of ice, the CIN measurements from the Citation and from the WB57F give extinctions a factor of 2–2.5 times higher than those derived from the particle data. We assume that these are overestimates because of particles[1] up in the FSSP and CAS probe inlets (Field et al. 2003) and the assumption of spherical small particles. There is the possibility of breakup on the leading edge of the CIN probe, but the manufacturer does not believe this to be a significant problem (H. Gerber 2005, personal communication). The difference in small size detection thresholds of the FSSP $\approx$ 2 μm is about the same as the CIN probe. In addition, because, as is shown in Figs. 2b and 3, the error is relatively independent of σ but the particle sizes that dominate the extinction increase with σ (see the end of section 2), errors resulting from probe mis-sizing are unlikely. Strapp et al. (2001) concluded for the 2DC probe they studied in the laboratory that relatively accurate size distributions can be obtained for sizes larger than about 125 μm. However, at smaller sizes the 2DC may undercount and mis-size (Korolev et al. 1998). Particles 125 μm and below sampled by the 2D imaging probe on the Citation contributed 9.3% $\pm$ 12.1% to the total extinction and for the WB57F was 19.7% $\pm$ 26%. In the unlikely event that half of the particles in this size range were not sampled by the 2DC imaging probes, the error would be equal to the values shown above. As a further check of the 2DC probe's sampling small particles, we compared the size distributions from the FSSP and 2DC probes for overlapping size ranges. The FSSP concentrations were larger by about a factor of 5 although there is considerable variability. The FSSP-shattered particles often end up in the largest size bin of the FSSP and may therefore be artifacts, thereby leading to higher concentrations at this end of the FSSP size distributions. The discrepancy noted between the direct and indirect estimates of extinction are not likely to be explained by errors in sizing and counting by the imaging probes. Finally, a compelling reason to consider σ from the particle probes preferable to σ from the CIN is because the extinction detection limit in particle probes ($<$0.0001 m^{-1}) is significantly lower than that from the CIN (0.0004 m^{-1}). Extinction values derived from the Lidar In-space Technology Experiment (LITE) instrument's measurements of backscatter for the period the lidar was operational (D. Winker 2005, personal communication) indicate that σ is almost always below 0.0004 m^{-1} when the lidar was transmissive to cloud (optical depths below about 5). It is essential to have instruments that measure very low values of extinction.

One goal of CRYSTAL-FACE has been to compare measurements from overflying aircraft with those measured in situ so that lidar, radar, and radiometric remote sensing retrieval algorithms can be developed and evaluated. In Figs. 5a and 5b, σ is estimated from the ER-2 lidar (McGill et al. 2004) and from the coincident CIN, and particle probe data from the Citation (on 19 and 23 July) and the WB57F (23, 26, and 29 July) are intercompared. For one of the two Citation cases (23

[1] We have removed particles imaged by the 2DC probe that are likely to be produced through shattering based on particle interarrival times, as described in FHB. This led to an average 6% decrease in the σ derived from the particle probes.

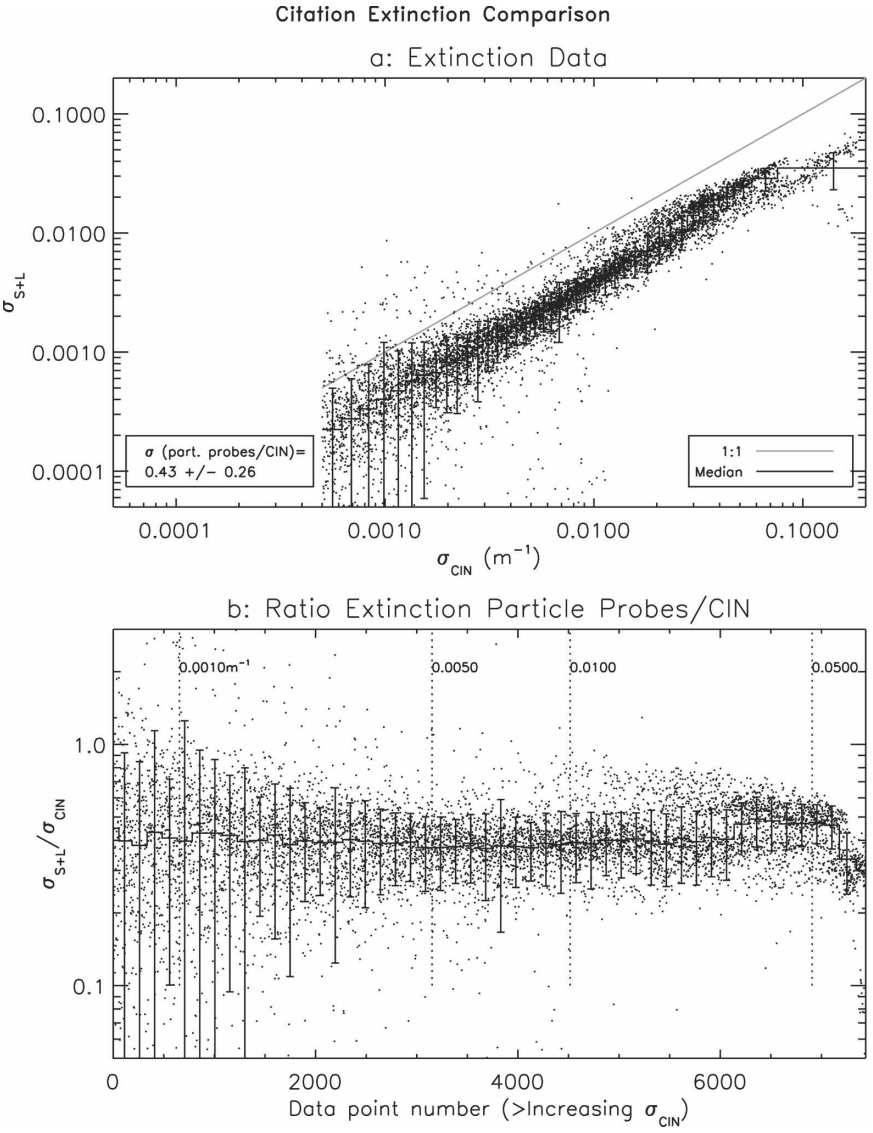

FIG. 3. Comparison of extinction derived from the FSSP (small particles) and imaging probe (large particle) (σ_{S+L}) to extinction derived from the CIN probe (σ_{CIN}). (a) σ_{S+L} vs σ_{CIN}. Data are from Citation aircraft during CRYSTAL-FACE. Shown are the 1:1 line and the histogram showing median values derived in 20 intervals, each with an equal number of data points. (b) Ratio of the two extinction values, sorted by increasing σ_{CIN}, with vertical lines showing σ_{CIN} values at selected x positions.

July) and most of the WB57F periods, it was possible to directly measure the height-dependent extinction, and the extinction at the aircraft's height, because the lidar beam was transmissive through the cloud layer to the ground or ocean surface (see McGill et al. 2003). Although the considerable scatter shown is to be expected because of the inevitable aircraft mismatch of times and locations, σ from the particle probes is correlated almost 1:1 with the lidar retrievals and σ from the CIN is larger by about a factor of 2. Although σ derived from lidar backscatter involves assumptions, these assumptions are not likely to account for a factor of 2 error.

We now turn our attention to the measurement of IWC, also a necessary variable in the estimation of r_e. The IWC from the WB57F is evaluated first because a new instrument was used: a Harvard total water instrument (Weinstock et al. 1994; Weinstock 2005, unpublished manuscript). This instrument measures total water during a brief (0.2 s) transit of air and condensate through an isokinetic heated inlet and out through an

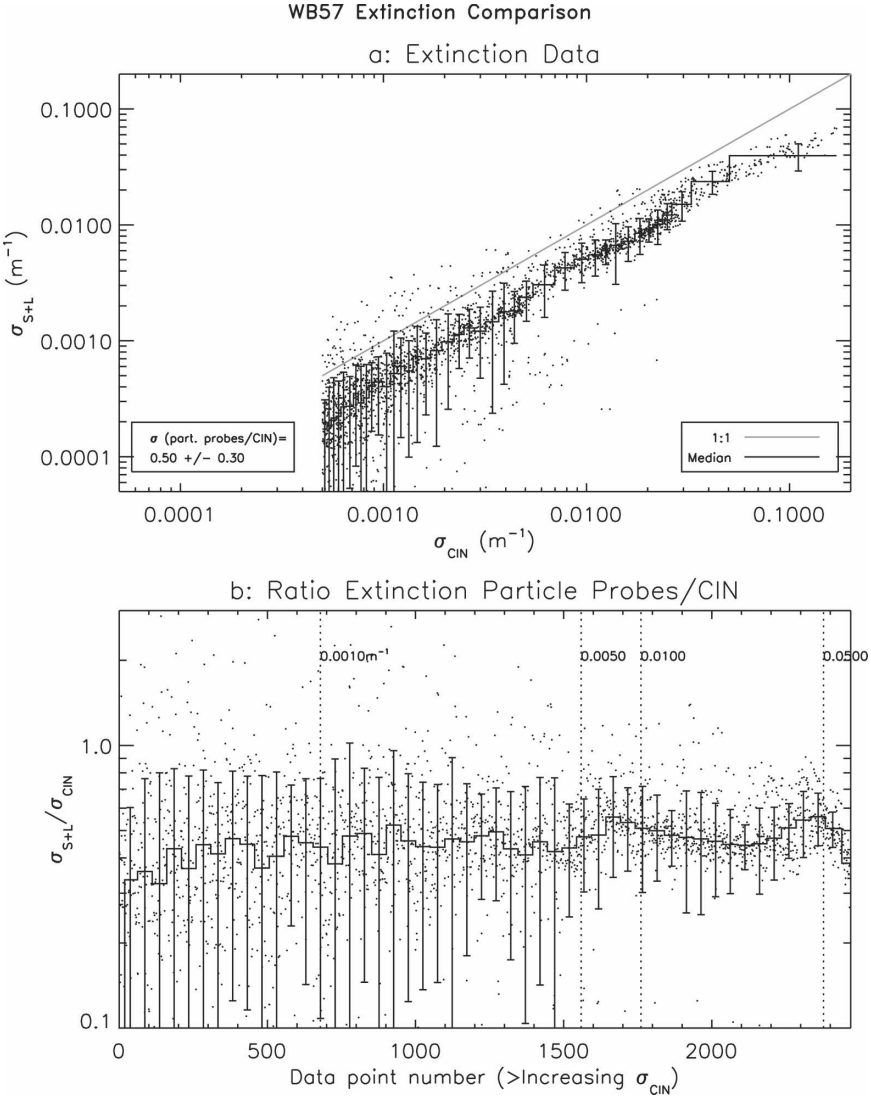

FIG. 4. Same as in Fig. 3, except with data from the WB57F aircraft during CRYSTAL-FACE, along with small particle data from the CAS probe and large particle data from the CIP probe.

exhaust port. The IWC is the difference between the total water and water vapor measured by a Harvard hygrometer (Weinstock et al. 1994). The Harvard instrument detection threshold is about 0.003 g m^{-3}. It appears to measure IWC accurately except in the presence of large particles, which it cannot fully sublimate (Heymsfield et al. 2004b). Figure 6 illustrates this difficulty where scattering as detected by an optical sensor in the instrument's exhaust port is related to the slope λ derived from the particle probes. The slope is essentially the inverse of the mean particle size (see Heymsfield et al. 2004a). When there are large particles (low λ) and a relatively high IWC, condensate streams out of the probe's outlet. This effect is further illustrated in Fig. 7, where the IWC calculated from the particle probe size distributions is small (from the CAS probe) and large (2D probe) sizes are compared to those measured by the Harvard instrument. The relationships used to convert particle size to mass use the density parameterization of Heymsfield et al. (2004a) with the additional assumption that all small particles are solid ice spheres. Although there is considerable scatter, on average the comparison is good except for those cases where the IWC > 0.01 g m^{-3}, coinciding with situations where large particles are present. This result suggests that r_e would be underestimated when the IWC measured from the WB57F were above about 0.01 g m^{-3}.

Several studies indicate that the counterflow virtual

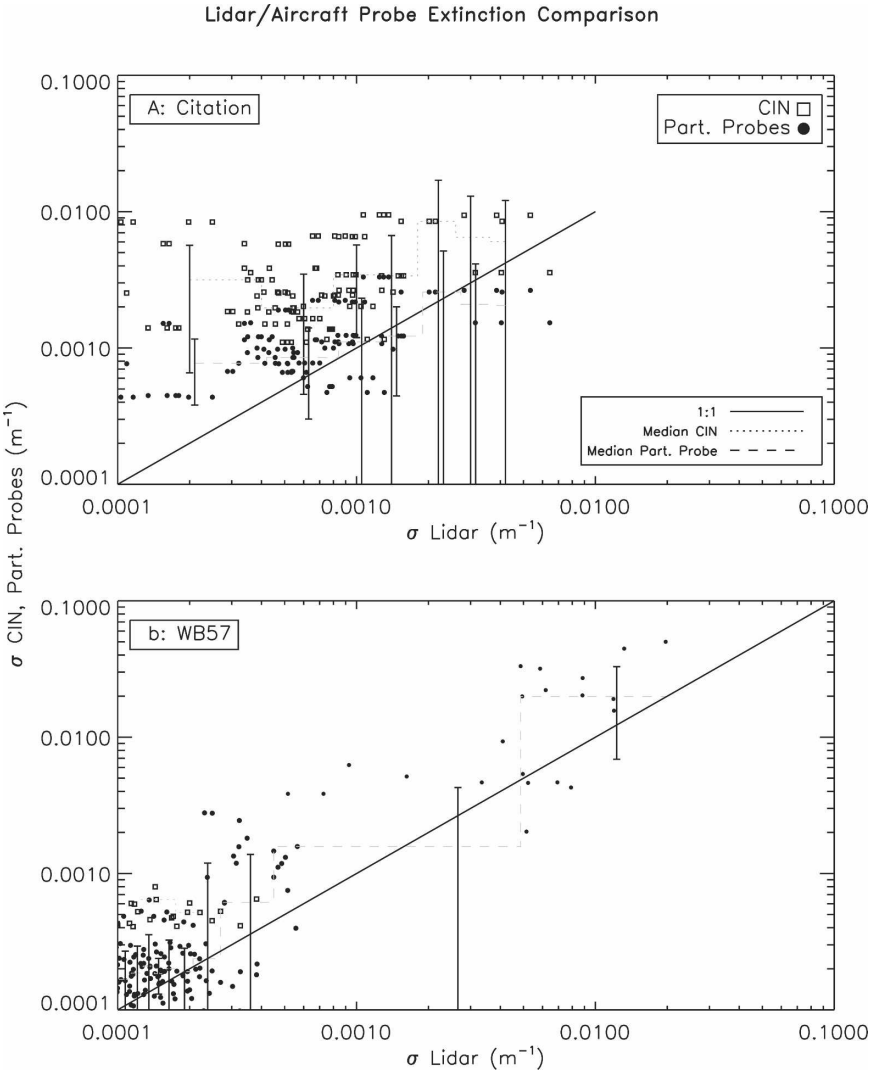

FIG. 5. Comparison of extinction deduced from CRYSTAL-FACE periods of collocations of ER-2 (lidar) and in situ particle probes from (a) Citation, on 19, 23, 28, and 29 Jul; and (b) WB57, on 23, 26, and 29 Jul.

impactor (CVI) provides accurate condensed water contents (Twohy et al. 1997) and this assertion is supported by the results shown in Fig. 2a and the appendix. Figure 8 shows the IWC derived from the small (FSSP) and the large [2DC + High Volume Precipitation Spectrometer (HVPS)] particle probes and the density formulation from Heymsfield et al. (2004a), again with the assumption that the small particles are solid ice spheres, compared with the IWC measured by the CVI from CRYSTAL-FACE. Overall, the comparison is excellent, a result to be expected because the formulation was developed using the CVI data. The particle probes therefore appear to give reasonably accurate IWC measurements throughout the range of IWC encountered. At IWCs larger than 1 g m^{-3}, the CVI can become saturated if its flow rates are not adjusted manually to compensate for the higher values. Additionally, ambient IWCs > 1 g m^{-3} usually corresponded to internal CVI water vapor concentrations outside the calibration range used during CRYSTAL-FACE and so are less accurate. In this high-IWC regime, IWCs derived from the particle probes are therefore especially valuable.

The estimation of [IWC/σ] from direct measurements can be compared with those derived from the particle probes with a clearer understanding of the limitations of the input variables. The IWC measured by the Harvard probe (IWC_{har}), divided by the σ measured by the CIN probe, σ_{CIN}, for the WB57F CRYSTAL-FACE observations is shown as a function of σ_{CIN} in Fig. 9a. Over the range of the measured IWC

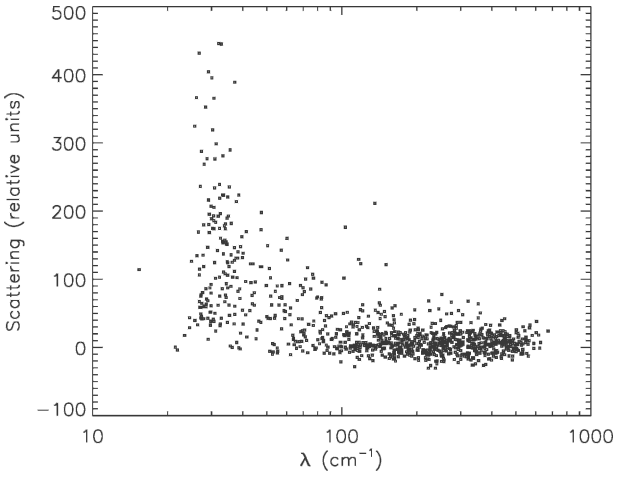

FIG. 6. Relative scattering detected in condensate in the exhaust of the Harvard total water content instrument as a function of the slope λ of the gamma distribution fitted to the size distributions measured by the CIP probe from the WB57F aircraft during CRYSTAL-FACE. (Harvard data courtesy E. Weinstock and J. Smith, Harvard University, Cambridge, MA.)

(dashed sloping lines), [IWC/σ] is relatively constant except where σ is low. Figure 9b shows the same data as in Fig. 9a, adding IWC_{har} for those instances where $\lambda < 80\ cm^{-1}$ (large particles). Figure 9c illustrates that when the particle probes are used to estimate IWC, [IWC/σ] increases monotonically with σ (Fig. 9c). This suggests that in [IWC/σ], σ is flat when derived from IWC_{har} because, for large values, IWC is underestimated. Figure 9d gives the particle probe data for IWC and σ. Here, because σ is about half as large, [IWC/σ] is much larger. The gray symbols on the left side in Fig. 9d show the points derived from the PSD where σ fell below the CIN detection threshold. Although the results suggest that [IWC/σ] is relatively constant for $\sigma < 0.0005\ m^{-1}$, it illustrates the need for σ measurements lower than those currently available from the CIN.

An assessment of the trend in [IWC/σ] as a function of σ, for temperatures warmer than those from the WB57F, can be made from the Citation measurements above the detection thresholds of the CVI ($IWC > 0.005\ g\ m^{-3}$) and the CIN ($\sigma > 0.0005\ m^{-1}$). The extension of σ to values larger than for the WB57F observations is presumably because of larger particles associated with warmer temperatures (Table 1). In Fig. 10a, [IWC/σ] is not as low because of the CVI's detection threshold. There is no clear trend of [IWC/σ] with σ, the average being about $15\ g\ m^{-1}$, around that from the WB57F data. At large σ, the dropoff of [IWC/σ] is an artifact attributable to the CVI's inability to detect IWC above about $1\ g\ m^{-3}$. In Fig. 10b, where IWCs are above and below the CVI's sampling range, IWCs from particles have been factored in. This addition further flattens the distribution of [IWC/σ] with σ. Exclusive use of the particle probe data results in a more realistic increase in [IWC/σ] with σ (see Heymsfield et al. (2003)—the values of [IWC/σ] being due to larger particles. When particle probe data are used, it is noted that [IWC/σ] increases with σ (Fig. 10c).

In CRYSTAL-FACE, the [IWC/σ] data from the CIN and particle probes can be further evaluated using lidar–radar retrievals of [IWC/σ] and appropriate modeling calculations. In the three panels of Fig. 11, the shaded regions illustrate the temperature dependence and variability of [IWC/σ] derived from remote sensing data. The data were collected at the Department of Energy Atmospheric Radiation Measurement (DOE/ARM) Southern Great Plains site (van Zadelhoff et al. 2004) and derived from a range of ice cloud types. Here, [IWC/σ] generally increases with temperature. Coincident lidar and radar data are required for the analysis given in Fig. 11. Because of this, the observed [IWC/σ] at lower temperatures is biased to larger values as exclusively small particle regions are not usually detectable by radars. At higher temperatures IWC is biased to optically thinner, nonanvil clouds that can be penetrated by lidar. These clouds are likely to have lower σ, lower radar reflectivity, lower IWC, and lower values for [IWC/σ]. Increasing temperature coincides with increasing [IWC/σ].

A particle growth model has been used to examine [IWC/σ] over a range of cirrus-forming temperatures (Fig. 11a). The model considers the growth of cloud condensation nuclei (CCN) from initialization at a relative humidity of 60% with respect to water, to the formation of haze particles and activation of cloud droplets, followed by homogeneous nucleation and subsequent growth. The particles are lifted slowly in parcels rising at 5 and 20 $cm\ s^{-1}$, characteristic of synoptically generated cirrus (Heymsfield et al. 2005). The particles are taken to be solid ice spheres for the extinction and growth rate calculations. These calculations do not consider ice particle fallout and are most relevant to early cirrus cloud formation or to the tops of cirrus layers where ice fallout from parcels is relatively small.[2]

In Fig. 11a, the change in [IWC/σ] with temperature begins at the parcel's initialization (X in the panels). Then, [IWC/σ] increases with time and decreasing temperature; IWC increases faster than σ. The [IWC/σ] levels out as the excess vapor density is depleted and

[2] The CCN distribution is largely immaterial because only a small portion of the CCN population freezes in these weak updrafts.

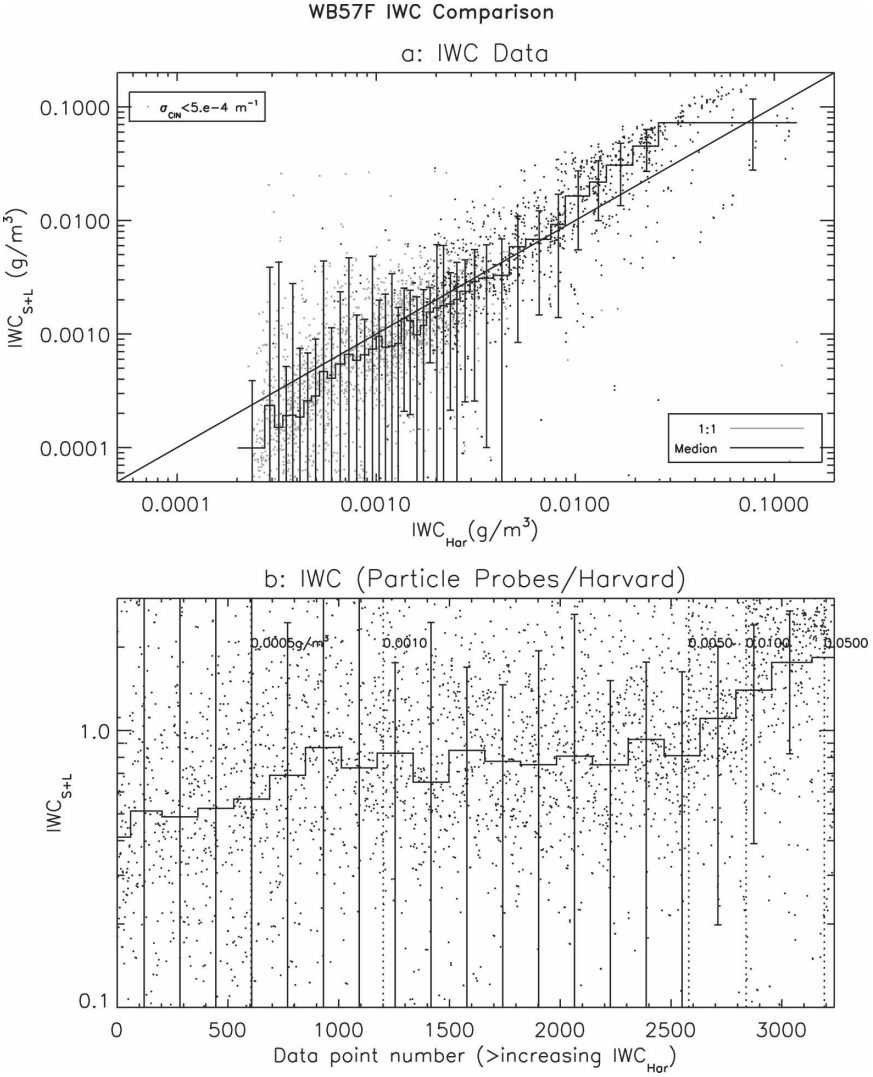

FIG. 7. Same as in Fig. 3, except for IWC, which is measured by the Harvard total water (IWC_{har}) and water vapor probes and is calculated from the size distributions.

growth essentially ceases. Its values are higher with weaker velocities and when heterogeneous nucleation (not considered here) is also operative, since fewer but larger particles are produced. The IWC is essentially governed by parcel lifting and σ is relatively large because temperature-dependent ice particle concentrations, 1–10 cm^{-3}, are about 10 times larger than are indicated from most observations in synoptically generated cirrus. The [IWC/σ] given here therefore represents its lower limit. The IWC in anvil cirrus will be up to an order of magnitude higher than that derived here because of the transport of ice mass from below and extinction at the lower temperatures. The model results therefore could apply to anvil ice cloud layers if shifted to the right by roughly a factor of 2.

In Fig. 11b, mean values of [IWC/σ] from the CIN probe on the WB57F and Citation aircraft are examined in temperature increments of 5°C. The IWCs are derived from the PSD because they cover the broadest range of IWCs and also remove issues related to incomplete sublimation of ice mass by the Harvard and CVI instruments.

In Fig. 11c, mean values of [IWC/σ] from the particle probes are plotted as a function of temperature. As in Fig. 11b, the IWCs derive from the PSD. In general, the [IWC/σ] values from the particle probes are at the larger end of the remote sensing data. This may not be surprising given that the CRYSTAL-FACE data are from thick, deep anvils with a likelihood of larger [IWC/σ] values than those sampled in the lidar–radar

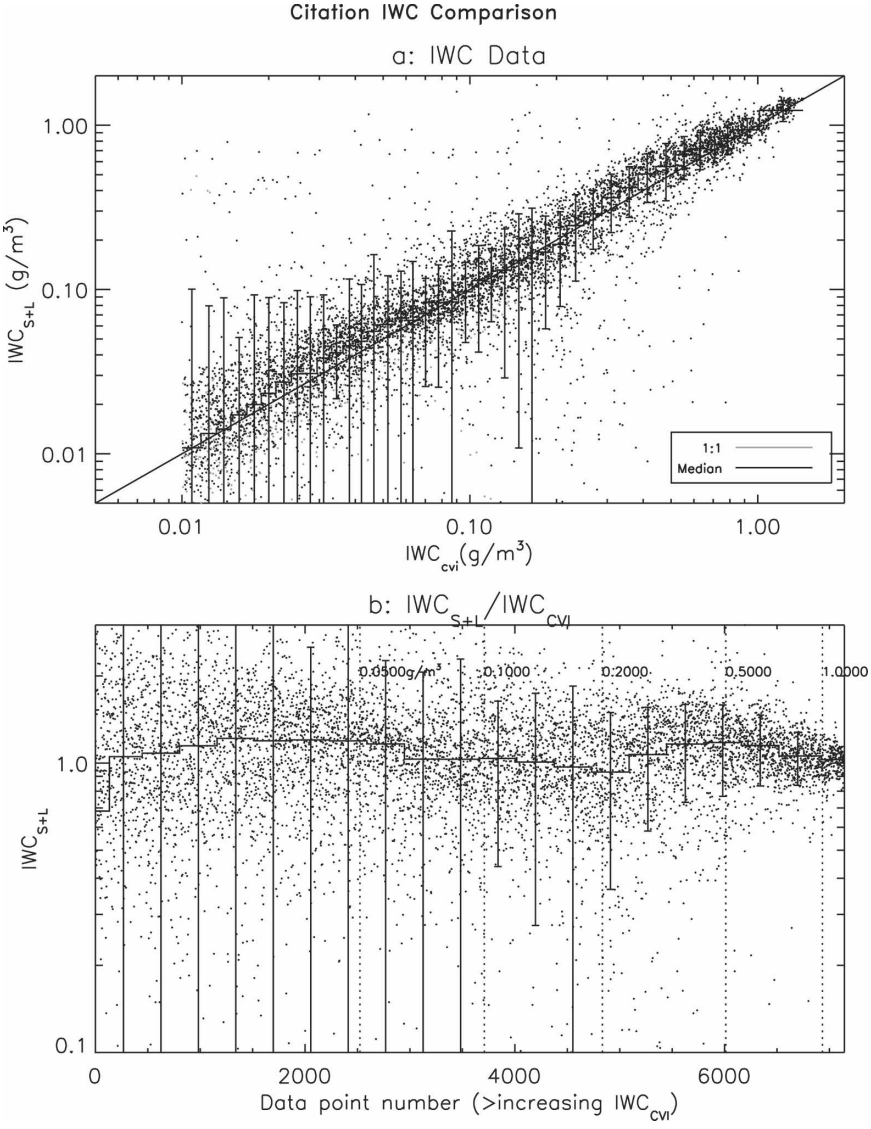

FIG. 8. Same as in Fig. 7, except for the Citation aircraft, where the condensed water content is measured by the CVI probe and the IWCs are calculated using the FSSP and imaging probe data.

approach. There may be other factors that influence the comparison as well.

Also in Fig. 11c, we show [IWC/σ] values derived from balloon-borne replicators in synoptically generated cirrus during the First International Satellite Cloud Climatology Program (ISCCP) Experiment (FIRE-2) and from thin cirrus during the Central Equatorial Pacific Experiment (CEPEX) where the video ice particle sampler (VIPS) provided excellent imagery of small ice particles. Temperatures sampled by the replicator spanned the range from $-65°$ to $-22°$C and 109 data points each spaced about 100 m in the vertical. The CEPEX data were obtained in the $-40°$ to $-48°$C range. These data are at the higher end of the [IWC/σ] values observed by the lidar–radar approach but are much lower than those observed from the CRYSTAL-FACE observations in appreciably thicker ice cloud.

The sizes that dominate extinction and the ice water content from CRYSTAL-FACE are further ascertained as a means of assessing whether our current suite of microphysical probes can adequately sample particles in critically important size ranges. We use the WB57F measurements of the size distributions and particle areas and estimates of particle masses measured with the particle probes, which for the FSSP assumes spherical particles. Taking the particle probe estimates of σ to be qualitatively correct, Fig. 12a shows that the

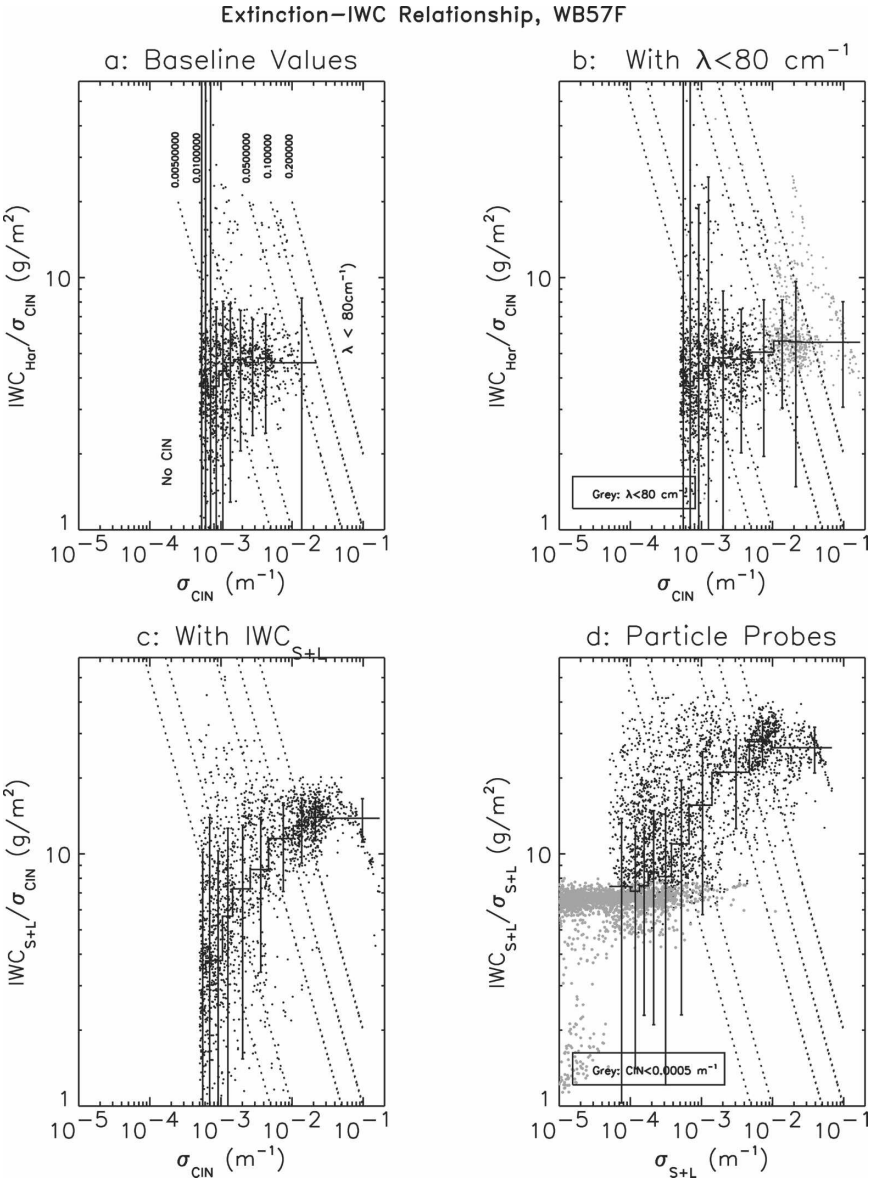

FIG. 9. Ratio of the ice water content to extinction as a function of extinction from WB57F measurements in CRYSTAL-FACE: (a) measurements; (b) as in (a), except including IWC measurements thought to be underestimated due to incomplete ice sublimation (gray symbols); (c) same as in (b), except using IWC derived from the particle probes at the times of incomplete sublimation; and (d) extinction derived from the particle probes. Gray points indicate the periods where particles are only small.

fraction of σ contained in sizes measured by the CAS probe is nearly unity at low values of σ but decreases with increasing σ. This observation is further clarified in Fig. 12b, which shows the diameter that divides in half the extinction values from the particle probe data (D_{ma}). When σ values are low, particles 20 μm and below provide almost half of the extinction. As σ increases, larger particles contribute more. The percentage of the IWC in small particles decreases monotonically with increasing particle size (Fig. 13a), leading to the result that, for IWC above about 0.01 g m^{-3}, more than half of the IWC is in large particles. This result is further demonstrated from the median mass diameters (D_{mm}) in Fig. 13b, where it is noted that particles 100 μm and above compose most of the ice condensate. These results would be amplified using data from lower levels in the storm, where increasing [IWC/σ] corresponds to increasing D_{mm} relative to D_{ma}.

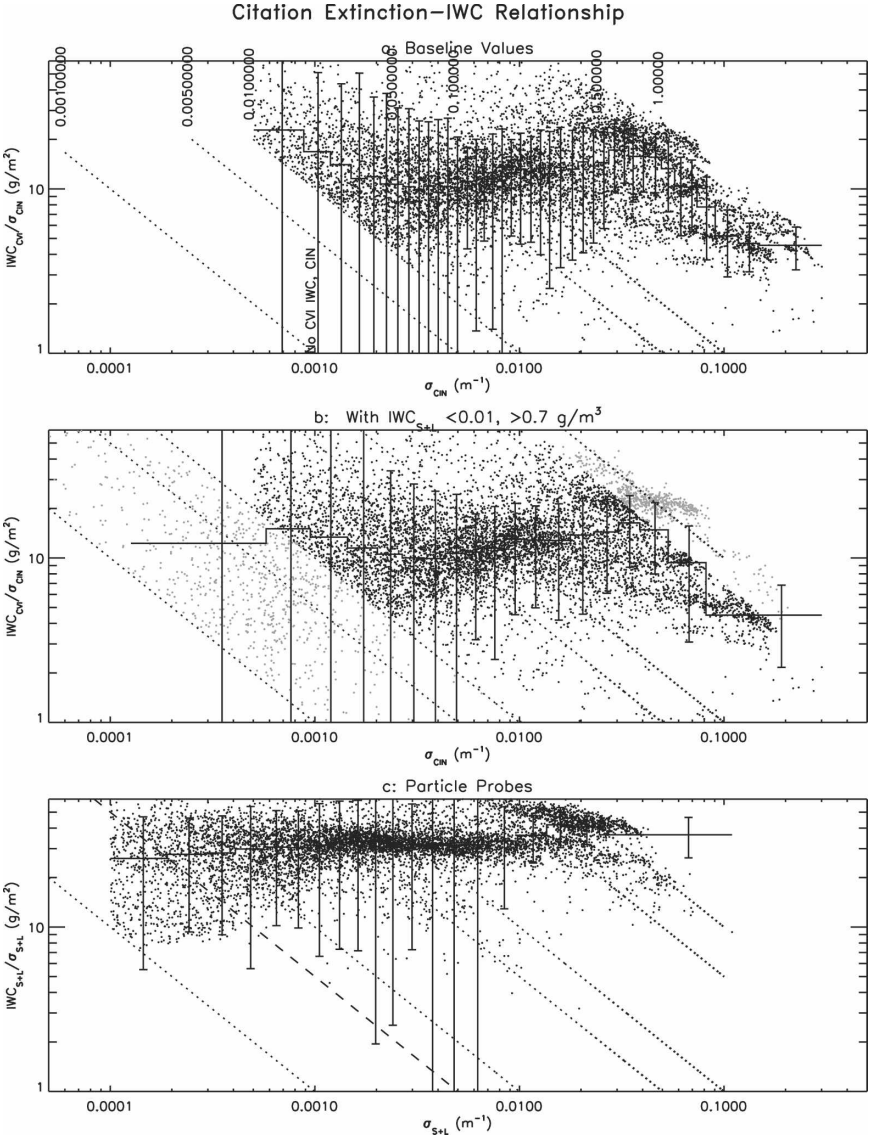

FIG. 10. Same as in Fig. 9, except from the Citation aircraft.

3. Observations in a wave cloud

Lenticular orographic wave clouds provide a quasi-steady thermodynamic and kinematic environment to observe and model ice cloud properties in a laboratory-like environment. On 5 May 2004, the WB57F flew from upwind to downwind in such a cloud over Colorado during the Midlatitude Cirrus Cloud Experiment (MidCiX). This cloud provided an environment to compare and evaluate IWC and σ from direct and indirect methods.

The horizontal updraft/downdraft extent of the wave was about 1.8 km and the WB57F penetrated the cloud just downwind of its leading edge, where the cloud rose to the aircraft's altitude. The sampling temperature was about -56°C, relative humidity was 76% with respect to water from the Jet Propulsion Laboratory (JPL) tunable laser diode hygrometer, peak vertical velocity from onboard measurements was about 0.5 m s^{-1} (P. Bui 2004, personal communication), horizontal wind velocity was 25 m s^{-1}, and mean wind direction was from 276°. The WB57F penetration was essentially along the airflow, about 13° off the mean wind direction, at a true airspeed of about 6 times the velocity of the horizontal wind. Peak concentrations from the FSSP and CAS operating on the WB57F were about 5 cm^{-3}.

The growth of particles in the cloud was simulated using the homogeneous nucleation model discussed in section 2. As noted, these calculations assume that the

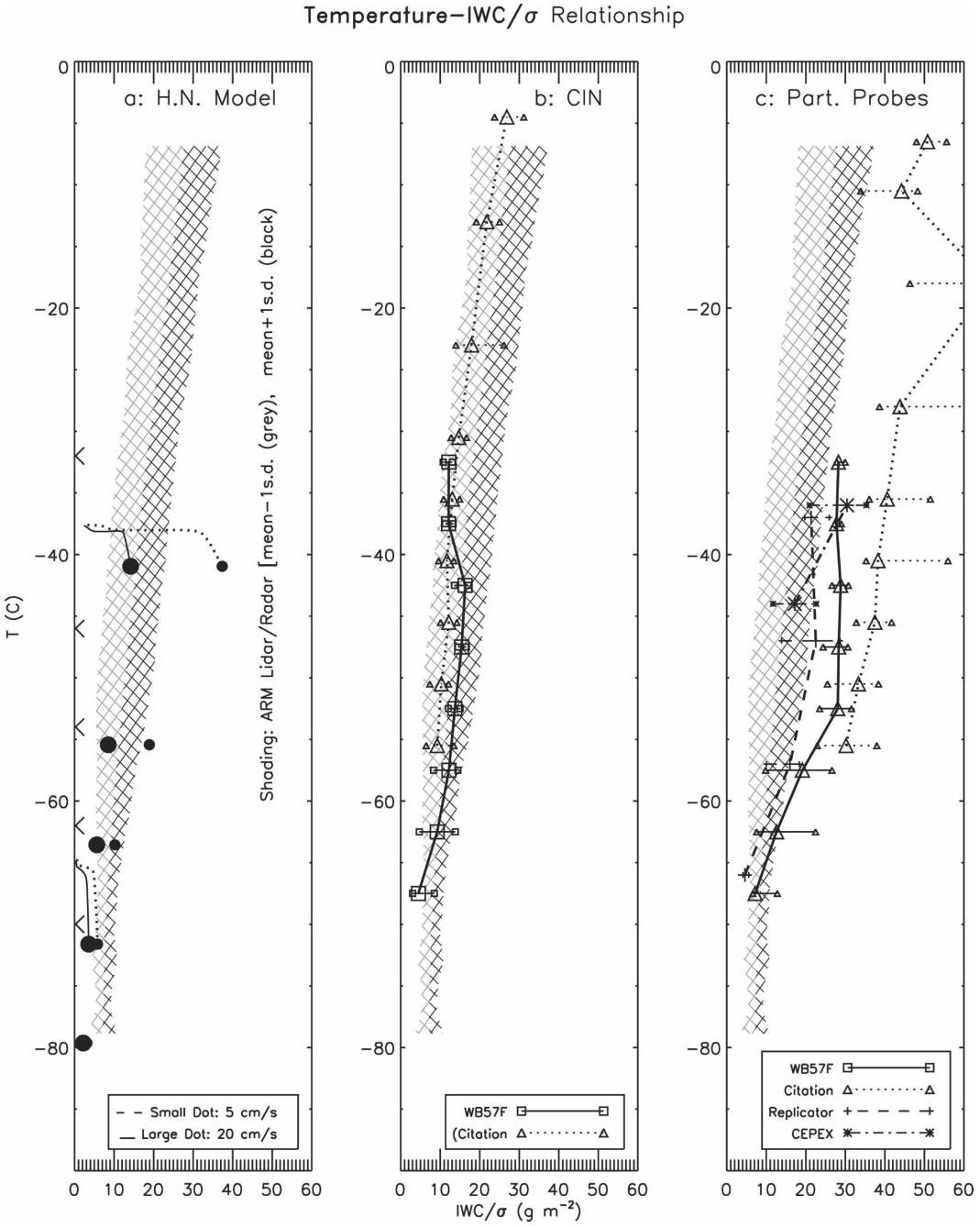

FIG. 11. Temperature dependence of [IWC/σ] as derived from (a) the homogeneous ice nucleation model, (b) CIN probe measurements during CRYSTAL-FACE, and (c) particle probe data from several field programs. The shaded region shows values derived from ARM lidar–radar retrievals and $\pm 1\sigma$ regions distinguished by shading.

particles are solid ice spheres, consistent with our VIPS observations for the sub-50-μm particles in this wave cloud. In the model, a constant vertical velocity of 0.5 m s^{-1} was used for simplicity, and the initial temperature was chosen such that it gave the same temperature and nearly the same relative humidity as measured on the WB57F by several precision hygrometers. Vertical velocities of 30 and 70 cm s^{-1} produced relative humidities at the aircraft level, which were much too low and somewhat too high. Given the vertical velocity and initial temperature, the resulting concentration of homogeneously nucleated ice was 6 cm^{-3}, close to the measured values.

Figure 14a compares the measured IWC from a

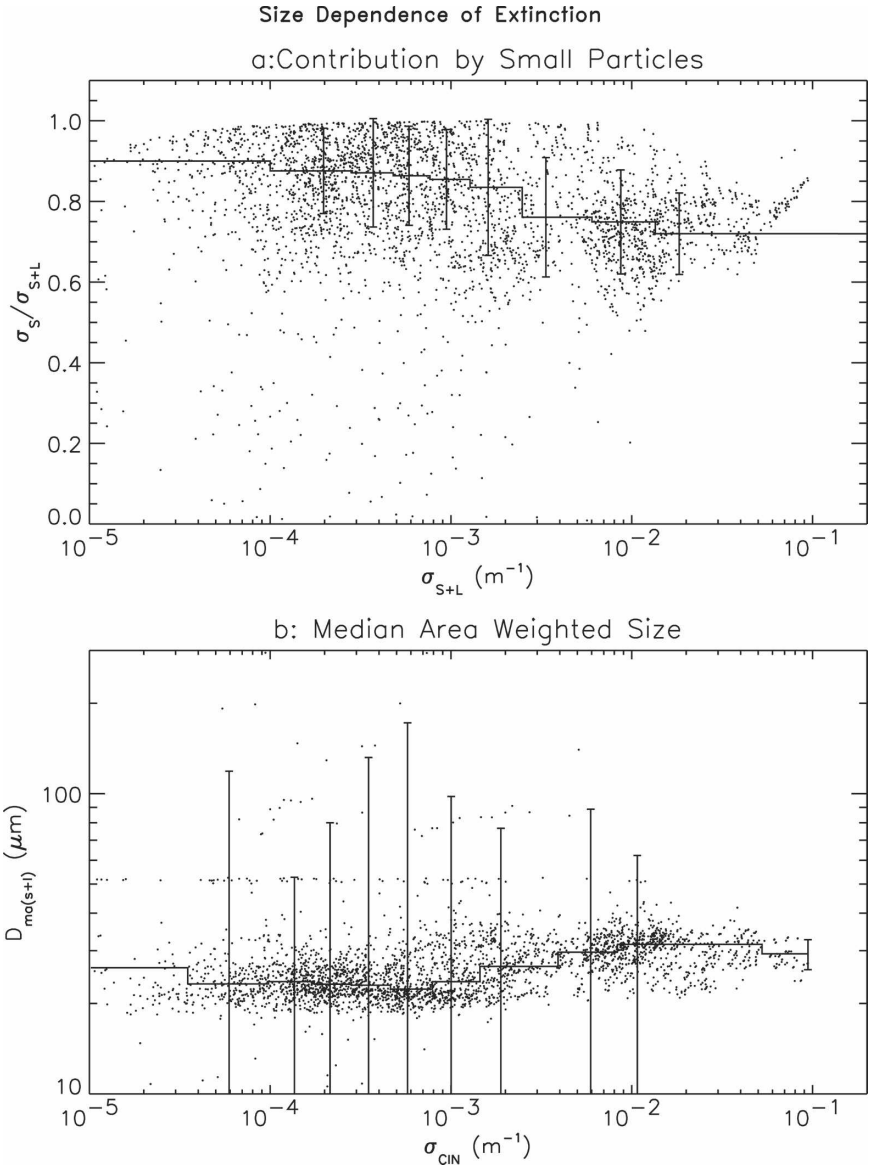

FIG. 12. Dominant particle sizes contributing to extinction, from WB57F observations. (a) The ratio of extinction in small (CAS) to all (CAS + CIP) sizes as a function of σ_{CIN}. (b) Median area-weighted particle size as a function of σ_{CIN}.

newly designed CVI, from FSSP and CAS probes assuming that the particles are solid ice spheres, and from the model. The model results shown in the figure are scaled in time to account for the factor of 6 difference between the horizontal wind and aircraft velocities. The model IWCs are quite robust in that they are primarily dependent upon how far the air parcel lifted from initialization and the relative humidity at each level and minimally to the assumption that the particles are solid ice spheres. Initially, the model IWC increases before the aircraft probes. Our VIPS operated on the WB57F and indicated particles as large as 40 μm at the first detection of FSSP and CAS particles. (VIPS data will be reported on in a later paper.) Therefore, the WB57F entered the cloud downwind of where it began. Within the cloud, there is excellent agreement between the CVI, FSSP, and model IWCs, whereas IWC from the CAS appears to be underestimated.

In Fig. 14b, it is noted that σ from the direct measurement is about twice as large as those indirectly derived. The model values fall below those from the CIN and above those derived from the particle probes. The model σ are dependent upon the assumed particle cross-sectional area and shape and represent an upper

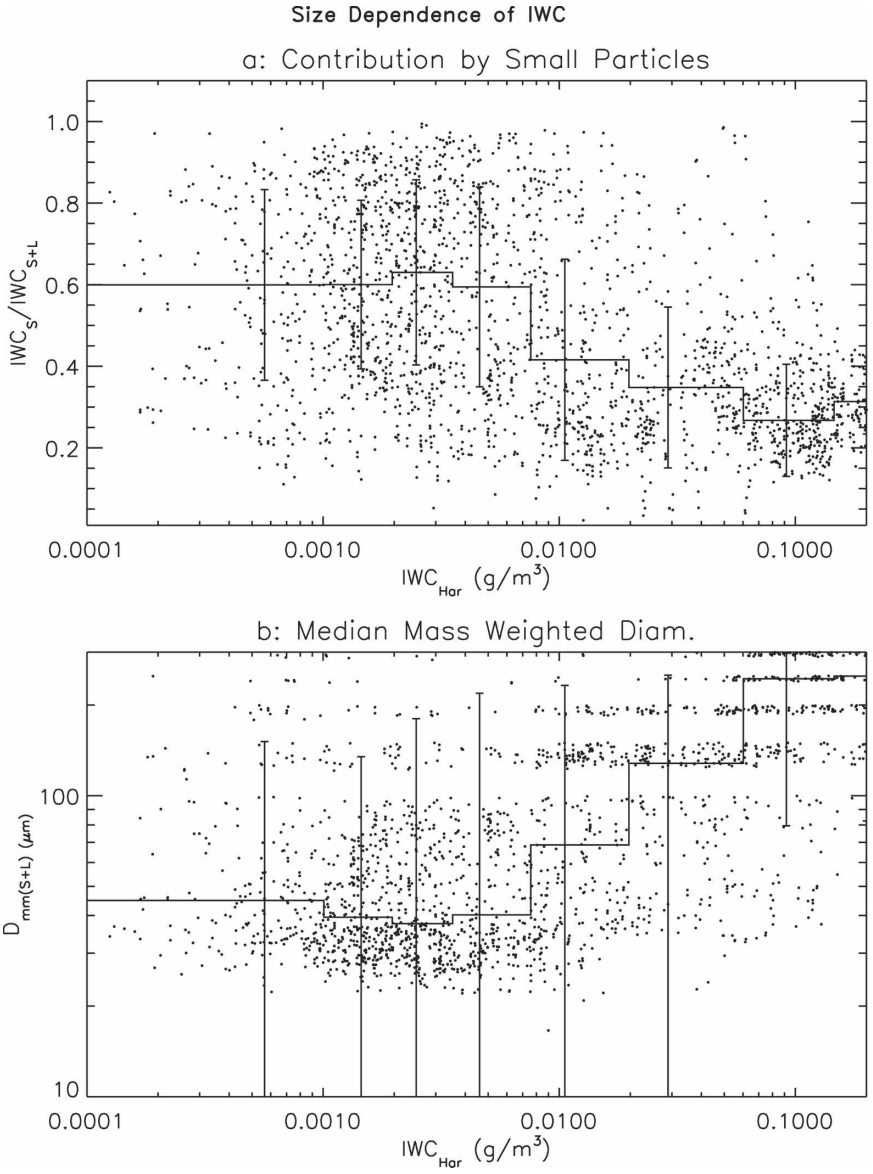

FIG. 13. Same as in Fig. 12, except for IWC.

limit because they are assumed to be spheres. Video ice particle sampler (VIPS) and cloud particle imager (CPI) data indicated the particles were quasi-spherical shapes with an "area ratio" (ratio of the particle area to the area of equivalent maximum diameter sphere) close to unity. Some of the largest particles were "budding rosettes" with an area ratio in the 0.6–0.7 range. The mean area ratio was within 10% or 20% of the assumed area ratio of unity. The modeled σ could be scaled downward by perhaps 10%–20% to conform more closely to the observation with little effect on the modeled growth of the particles. Therefore, the data from the particle probes conform relatively well to the model results.

4. Summary and conclusions

Using coincident measurements of extinction, ice water content, particle size distribution, and particle habit information from probes mounted on midlevel and upper-level aircraft during CRYSTAL-FACE and in MidCiX, we have evaluated the attributes and relative accuracy of various means of obtaining the ratio [IWC/σ], proportional to the effective radius. It is found that σ measured by the cloud-integrating nephelometer probe is systematically larger than σ from particle size distribution data for small (<50 μm) and large (50 to >1000 μm) sizes by a factor of about 2 (WB57F) or about 2.5 (Citation), whether in ice regions or in regions domi-

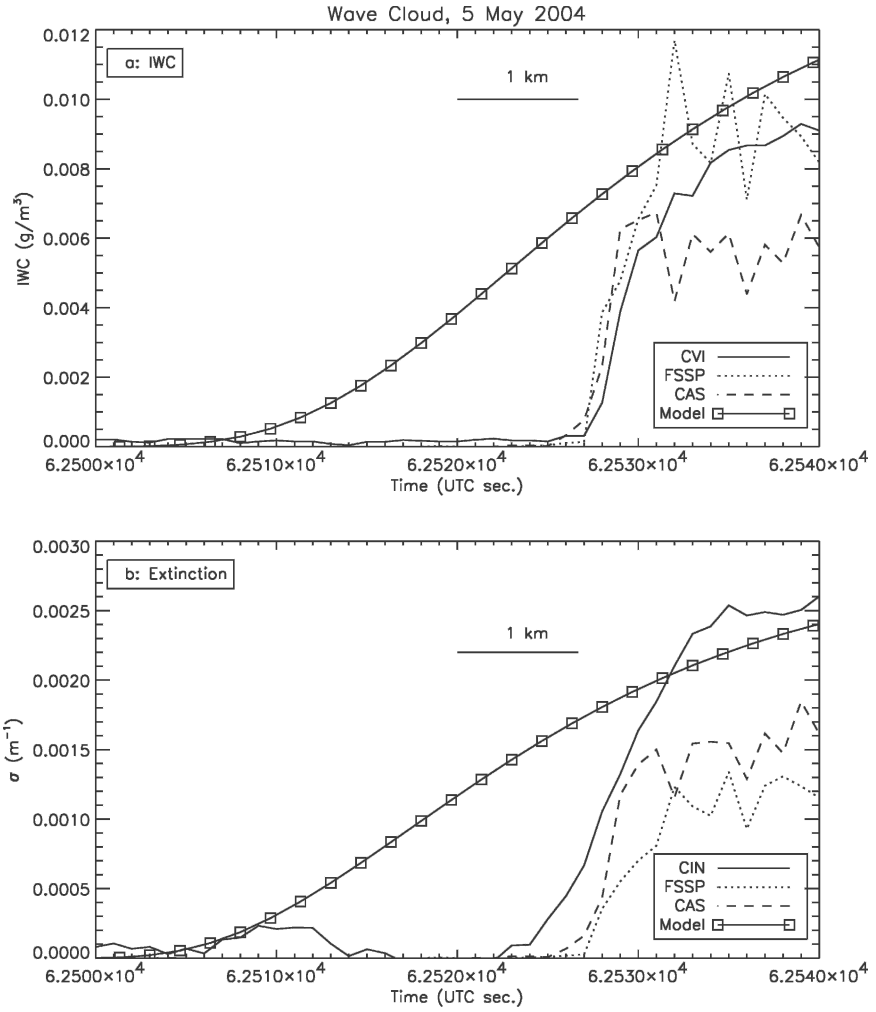

FIG. 14. Measurements from WB57F in an orographic wave cloud over CO during MidCiX and homogeneous nucleation model results: (a) ice water content and (b) extinction.

nated by cloud droplets (Citation). Because of their detection threshold, the CIN data are from regions of relatively optically thick cloud, especially for lidar probing, and therefore the estimates of σ from the PSD are more desirable because they provide useful information in regions of optically thin cloud.

Because of this discrepancy, H. Gerber (2004, personal communication) evaluated the calibration of the CIN using a collocated transmissometer operating in a mountaintop cloud sampling at the local wind speed. He concluded that the CIN extinction coefficient is accurate to within 5%. Although Gerber argues that the high correlation noted between the CIN and particle probe estimates of extinction in clouds with differing particle characteristics suggests that breakup effects are not significantly influencing the CIN extinction values, this potential source of error could not be evaluated from the ground-based observations. Both the FSSP probe and the 2DC probe have significant artificially enhanced concentrations of small particles in regions where large particles are present (Field et al. 2003, FHB), as was the case for many of the CRYSTAL-FACE clouds. Because the CIN probe's frontal area exposed to ice particles is far larger than for the particle probes, we suggest that ice particle breakup on the CIN probe's inlet accounts for much of the discrepancy and data from this probe should be used with caution.

In CRYSTAL-FACE, the IWC measured by the Harvard (WB57F) or CVI (Citation) evaporator probes and directly from the PSD and mass–dimension relationships conform closely. This is to be expected because the mass to diameter relations are based on direct measurements. The indirect approach provides more reliable results in higher IWC, and larger particle regions where the evaporator devices are either saturated or cannot adequately sublimate the large particles. In

MidCiX, where the studied cloud was composed only of small particles, the direct, indirect, and model IWCs conform closely but the σ show factor of 2 differences.

Given that σ from the direct method is larger than from the indirect methods, estimates of [IWC/σ] and r_e are a factor of 2–2.5 smaller than when using the particle probe data. This finding is consistent with the findings of Garrett et al. (2003) who used the CIN data to assert that the effective radius of ice cloud layers is considerably smaller than previously derived from indirect methods. In any event, depending upon which approach to deriving r_e is correct, the implications for climate modeling are important.

Although there is no direct measurement of [IWC/σ] by which we can assess the absolute accuracy of the direct (CIN, CVI, or Harvard) and indirect (particle probe) methods, we are able to draw several inferences from the following results.

- In regions of liquid water where there was good agreement between the condensed water content derived from the PSD and that from the CVI, σ from the CIN were 2.5 larger than those from the PSD. The CIN σ in CRYSTAL-FACE ice regions were also 2–2.5 times as large as for the PSD.
- A similar conclusion is reached from extinction estimates from CRYSTAL-FACE ER-2 lidar measurements collocated with Citation and WB57F overflights.
- In a wave cloud where there was good agreement between the ice water content derived from the homogeneous nucleation model, from PSD, and those from the CVI, σ from the CIN were 2.5 times larger than those from the PSD and higher than those from the model. Closer agreement is obtained if our observations of particle shape from the VIPS probe are factored into the model.
- The temperature dependence of [IWC/σ], measured using CIN for σ in the vertically thick and high IWC CRYSTAL-FACE cloud layers, falls at the low end of those for comparatively thin cirrus derived using a combined lidar–radar retrieval scheme. Those derived from the particle probe data fall at the upper end.
- The temperature dependence of [IWC/σ] observed at the lower temperatures from the WB57F are consistent with those from the lidar–radar approach, but at low temperatures the latter are probably biased low. The [IWC/σ] derived from the particle probes are higher, but it is difficult to ascertain from this analysis alone whether the direct or indirectly derived [IWC/σ] are more accurate.
- A model, which treats the homogeneous nucleation of ice particles in parcels undergoing the weak ascent characteristic of synoptically generated cirrus at −32°C and below, showed a temperature dependence that was similar to the [IWC/σ] observed from the lidar–radar approach. The latter were sampled primarily in synoptically generated midlatitude cirrus. However, we conjecture that there is more ice mass than extinction added in outflow cirrus, and larger [IWC/σ].

It is clear from this analysis and the importance of the effective radius in climate model studies that an effort should be made to uncover the source of the discrepancies found in this study. Systematic intercomparison should be made in liquid water regions where particle shape, particle breakup, and the index of refraction errors are not likely to be significant. Additional observations should be done in cold, orographic wave clouds as well, where the physics of how particles grow and use up the available moisture are understood and can be modeled. We also point out that the use of particle probe data to derive [IWC/σ] is problematical because the sizes that dominate the IWC are in a range measured by the 2D imaging probes whereas those for extinction are sizes suited for the FSSP or similar probes. A number of potential sources of error can result when different probes with different sensitivities, sources of error, and sampling issues are used to obtain different measurements.

Acknowledgments. This research was supported by the NASA CRYSTAL-FACE program and MidCiX through NASA–NSF Agreement W-10, 024 (Hal Maring, program manager), and the Mesoscale and Microscale Division of NCAR. The authors are indebted to the crew of the UND Citation and NASA WB57F aircraft. Data from MidCiX was made possible through the efforts of Jay Mace, Paul Bui, and Paul Lawson. We express our deep appreciation to Tim Garrett, Hermann Gerber, and Nancy Knight for their thoughtful reviews of this manuscript.

APPENDIX

Counterflow Virtual Impactor

Condensed water content measurements were made using a counterflow virtual impactor on the Citation aircraft during CRYSTAL-FACE and a derivative of the CVI on the WB57F aircraft during MidCiX. The CVI water vapor sensor (Lyman-alpha or tunable diode laser hygrometer) is calibrated using a Licor LI-610 portable dewpoint generator. The LI-610 dewpoint value is traceable to National Institute of Standards and

Technology (NIST) standards and has an accuracy of 0.2°C. Pure nitrogen gas is used as a zero calibration source. Calibrations are performed at a wide range of dewpoints (humidities) and pressures from about 800 to 200 mb. At each pressure, a second-order polynomial fit for corrected absolute humidity as a function of sensor signal output is developed. The pressure dependence is then accounted for by generating another polynomial fit (as a function of pressure) for each of the coefficients in the first polynomial fit. Adjustments in the baseline offset are made on a flight-by-flight basis.

The above calibration procedure ensures an accurate determination of water vapor concentration inside the CVI upon evaporation of ice crystals. Since crystals are impacted into dry air, this is equivalent to the ice water content of crystals collected by the CVI. This is converted to ambient ice water content using an enhancement factor, which is based on the inertial enhancement of particles by the inlet. The collection characteristics of the CVI inlet can be predicted by simple theoretical calculations, which have been shown to be accurate through ground-based calibrations (Noone et al. 1988; Schwarzenbck and Heintzenberg 2000). Collection characteristics are based on particle aerodynamic diameter, so ice crystals will be sampled as efficiently as water droplets of equivalent aerodynamic size. Uncertainty for the CVI IWC can be estimated using a root-sum-square approach (Twohy et al. 1997). Uncertainties for CRYSTAL-FACE data are 13% at 0.5 g m^{-3} and 24% at 5 mg m^{-3}, while for MidCix data they range from 11% at 0.5 g m^{-3} to 15% at 5 mg m^{-3}.

In MidCix, IWCs measured by the CVI were compared to those measured by the Harvard total water instrument, which uses an isokinetic inlet and a fluorescence detection technique. Although some systematic differences were observed at very low IWCs, the two instruments generally agreed within about 10 mg m^{-3} from 0 to 100 mg m^{-3}. Additionally, the CVI data agree quite well with IWCs calculated from 2D imaging probe data processed using the latest techniques [two-parameter approach; Heymsfield et al. (2004a)].

REFERENCES

Boudala, F. S., G. A. Isaac, Q. Fu, and S. G. Cober, 2002: Parameterization of effective ice particle size for high latitude clouds. *Int. J. Climatol.,* **22,** 1267–1284.

Donovan, D. P., 2003: Ice-cloud effective particle size parameterization based on combined lidar, radar reflectivity, and mean Doppler velocity measurements. *J. Geophys. Res.,* **108,** 4573, doi:10.1029/2003JD003469.

Field, P. R., R. Wood, P. R. A. Brown, P. H. Kaye, E. Hirst, R. Greenaway, and J. A. Smith, 2003: Ice particle interarrival times measured with a fast FSSP. *J. Atmos. Oceanic Technol.,* **20,** 249–261.

Fu, Q., 1996: An accurate parameterization of the solar radiative properties of cirrus clouds for climate models. *J. Climate,* **9,** 2058–2082.

Garrett, T. J., H. Gerber, D. G. Baumgardner, C. H. Twohy, and E. M. Weinstock, 2003: Small, highly reflective ice crystals in low-latitude cirrus. *Geophys. Res. Lett.,* **30,** 2132, doi:10.1029/2003GL018153.

Gerber, H., V. Takano, T. J. Garrett, and P. V. Hobbs, 2000: Nephelometer measurements of the asymmetry parameter, volume extinction coefficient, and backscatter ratio in Arctic clouds. *J. Atmos. Sci.,* **57,** 3021–3034.

Heymsfield, A. J., and C. M. R. Platt, 1984: A parameterization of the particle size spectrum of ice clouds in terms of the ambient temperature and ice water content. *J. Atmos. Sci.,* **41,** 846–855.

——, and G. M. McFarquhar, 1996: On the high albedos of anvil cirrus in the tropical Pacific warm pool: Microphysical interpretations from CEPEX and from Kwajalein, Marshall Islands. *J. Atmos. Sci.,* **53,** 2424–2451.

——, S. Matrosov, and B. Baum, 2003: Ice water path–optical depth relationships for cirrus and deep stratiform ice cloud layers. *J. Appl. Meteor.,* **42,** 1369–1390.

——, A. Bansemer, C. G. Schmitt, C. Twohy, and M. R. Poellet, 2004a: Effective ice particle densities derived from aircraft data. *J. Atmos. Sci.,* **61,** 982–1003.

——, C. G. Schmitt, A. Bansemer, D. Baumgardner, E. M. Weinstock, J. T. Smith, and D. Sayres, 2004b: Effective ice particle densities for cold anvil cirrus. *Geophys. Res. Lett.,* **31,** L02101, doi:2003GL018311.

——, L. M. Miloshevich, C. Schmitt, A. Bansemer, C. Twohy, M. R. Poellot, A. Fridlind, and H. Gerber, 2005: Homogeneous ice nucleation in subtropical and tropical convection and its influence on cirrus anvil microphysics. *J. Atmos. Sci.,* **62,** 41–64.

Ivanova, D., D. L. Mitchell, W. P. Arnott, and M. Poellot, 2001: A GCM parameterization for bimodal size spectra and ice mass removal rates in mid-latitude cirrus clouds. *Atmos. Res.,* **59,** 89–113.

Korolev, A. V., J. W. Strapp, and G. A. Isaac, 1998: Evaluation of the accuracy of PMS optical array probes. *J. Atmos. Oceanic Technol.,* **15,** 708–720.

——, ——, ——, and A. N. Nevzorov, 1999: In situ measurements of effective diameter and effective concentrations. *J. Geophys. Res.,* **104,** 3993–4003.

——, G. A. Isaac, I. P. Mazin, and H. W. Barker, 2001: Microphysical properties of continental clouds from in situ measurements. *Quart. J. Roy. Meteor. Soc.,* **127,** 2117–2151.

McFarquhar, G. M., and A. J. Heymsfield, 1996: Microphysical characteristics of three cirrus anvils sampled during the Central Equatorial Pacific Experiment (CEPEX). *J. Atmos. Sci.,* **53,** 2401–2423.

McGill, M. J., D. L. Hlavka, W. D. Hart, E. J. Welton, and J. R. Campbell, 2003: Airborne lidar measurements of aerosol optical properties during SAFARI-2000. *J. Geophys. Res.,* **108,** doi:10.1029/2002JD002370.

——, and Coauthors, 2004: Combined lidar–radar remote sensing: Initial results from CRYSTAL-FACE. *J. Geophys. Res.,* **109,** D07203, doi:10.1029/2003JD004030.

Noone, K. J., J. A. Ogren, J. Heintzenberg, R. J. Charlson, and D. S. Covert, 1988: Design and calibration of a counterflow

virtual impactor for sampling of atmospheric fog and cloud droplets. *Aerosol Sci. Technol.,* **8,** 235–244.

Ou, S., and K.-N. Liou, 1995: Ice microphysics and climate temperature feedback. *Atmos. Res.,* **35,** 127–138.

Schwarzenbck, A., and J. Heintzenberg, 2000: Cut size minimization and cloud element break-up in a ground-based CVI. *J. Aerosol Sci.,* **31,** 477–489.

Strapp, J. W., F. Albers, A. Reuter, A. V. Korolev, U. Maixner, E. Rashke, and Z. Vukovic, 2001: Laboratory measurements of the response of a PMS OAP-2DC. *J. Atmos. Oceanic Technol.,* **18,** 1150–1170.

Twohy, C. H., A. J. Schanot, and W. A. Cooper, 1997: Measurement of condensed water content in liquid and ice clouds using an airborne counterflow virtual impactor. *J. Atmos. Oceanic Technol.,* **14,** 197–202.

van Zadelhoff, G.-J., D. P. Donovan, H. Klein Baltink, and R. Boers, 2004: Comparing ice cloud microphysical properties using CloudNET and Atmospheric Radiation Measurement Program data. *J. Geophys. Res.,* **109,** DC24014, doi:1029/2004JD004967.

Weinstock, E. M., and Coauthors, 1994: New fast response photofragment fluorescence hygrometer for use on the NASA ER-2 and the Perseus remotely piloted aircraft. *Rev. Sci. Instrum.,* **65,** 3544–3554.